Relativistic spin-polarized electronic structure of Ce and Pu

G. Schadler and P. Weinberger
Institut für Technische Elektrochemie, Technische Universität Wien, Getreidemarkt 9, 1-1060 Wien, Austria and Center of Materials Science, Los Alamos National Laboratory, University of California, Los Alamos, New Mexico 87545

A. M. Boring and R. C. Albers
Los Alamos National Laboratory, University of California, Los Alamos, New Mexico 87545
(Received 4 February 1986)

The first fully relativistic calculations that also include spin polarization are presented for the single-site t matrix for Ce and Pu. The pattern of resonant energies for Ce are compared to recent atomic eigenvalue results for the Ce^{3+} ion. The Ce band states are also determined along the $\langle 100 \rangle$ and $\langle 111 \rangle$ directions in the Brillouin zone by solving the Dirac equation with an internal magnetic field constructed from scalar relativistic linear muffin-tin orbital (LMTO) spin-polarized calculations. In the relativistic case the coupling between spin-orbit and spin-polarization interactions destroys rotational symmetry, unlike in the nonrelativistic spin-polarized formalism, and hence leads to completely nondegenerate f and d states in these systems (similar to the Zeeman effect). To see this we also give results for an applied magnetic field that only couples to the spins and hence resembles an effective internal spin-polarized field.

I. INTRODUCTION

The electronic structure of rare earth and actinide systems has become the subject of increasing scientific interest in recent years. In particular, the heavy-fermion systems have brought new excitement to this field of research, especially on the experimental side. The theoretical side, however, has been less satisfactory. Even if we ignore many-body effects, current theory usually neglects the problem that rare-earth and actinide systems require a fully relativistic treatment, yet often have strong tendencies towards local magnetism. Typically, self-consistent electronic structure calculations have emphasized one aspect or the other: They have either been fully relativistic with no account for spin-polarization effects or have been carried out in a spin-polarized mode using the Pauli-Schrödinger—like equation with spin-orbit coupling excluded. In the last few years the formal theory of spin-polarization in Dirac theory[1] has progressed, and the gap between the two approaches bridged by the methods of Strange *et al.*,[2] Feder *et al.*,[3] and Cortona *et al.*[4] Since experience has shown that relativistic effects are important even for $4d$-electron systems (e.g., see Ref. 2), this is an important theoretical achievement. As was shown by Strange *et al.*,[2] for $5d$-electron systems the effects of spin-polarization for relativistic single-site scattering are large. In particular, spin-polarized relativistic scattering seems to be important whenever sharp resonances in the vicinity of the Fermi energy characterize the electronic structure. As might be expected, large spin-polarization effects for $4f$ electrons were also found by Cortona *et al.*[4] for isolated rare-earth ions.

In the present paper the method of Strange *et al.*[2] is applied to the fully relativistic single-site scattering t matrix for cerium and plutonium. For Ce these single-site t matrices are then used to calculate relativistic spin-polarized energy bands along the $\langle 100 \rangle$ and $\langle 111 \rangle$ directions. The main effect is for the spin-polarization to remove any remaining degeneracy in the fully relativistic states.

For completeness the theoretical concepts are briefly summarized in Sec. II (for more details the reader is referred to Strange *et al.*[2]). In addition we also give new results for the formulation of the relativistic spin-polarized Korringa-Kohn-Rostoker (KKR) Green's function in terms of the single-site scattering operator. Computational details are presented in Sec. III. In Sec. IV the results are given and conclusions discussed in Sec. V.

II. THEORETICAL CONCEPTS

Strange *et al.*[2] have recently shown that the radial amplitudes of the Lippman-Schwinger equation for a Kohn-Sham-Dirac Hamiltonian in the presence of an effective magnetic field $\mathbf{B}_{\rm eff}(\mathbf{r})$, with both the effective potential $V_{\rm eff}(\mathbf{r})$ and $\mathbf{B}_{\rm eff}(\mathbf{r})$ spherically symmetric and the z direction in spin space to be taken along $\mathbf{B}$, can be determined by the following coupled set of radial differential equations:

$$\left[-\frac{\partial}{\partial r}+\frac{(\kappa'-1)}{r}\right] f_{QQ'}(r,E)+[V_{\rm eff}(r)-E+1]g_{QQ'}(r,E)+B_{\rm eff}(r)\sum_{\kappa''} G(\kappa'',\kappa,\mu)g_{Q''Q'}(r,E)=0\ , \tag{1}$$

 ©1986 The American Physical Society

$$\left[-\frac{\partial}{\partial r}+\frac{(\kappa'+1)}{r}\right]g_{QQ'}(r,E)+[V_{\text{eff}}(r)-E-1]f_{QQ'}(r,E)-B_{\text{eff}}(r)\sum_{\kappa''}G(-\kappa'',-\kappa,\mu)f_{Q''Q'}(r,E)=0\ , \tag{2}$$

$$B_{\text{eff}}(r)=\frac{e\hbar}{2mc}\left[B_{\text{ext}}+\frac{\delta E_{\text{xc}}[n,m]}{\delta \mathbf{m}(r)}\right]\ , \tag{3}$$

$$Q=(\kappa\mu)\ . \tag{4}$$

In Eq. (3) $\delta E_{\text{xc}}[n,m]/\delta\mathbf{m}(r)$ is the internal magnetic field as given by the local density functional,[5] B_{ext} is an external field that only couples to the spins, and n and m are the charge and magnetization densities. The dominant coupling[2] in Eqs. (1) and (2) is for values of κ belonging to the same value of l [$j=l+\frac{1}{2}(\kappa=-l-1)$, $j=l-\frac{1}{2}(\kappa=l)$]. In this case the coefficients $G(\kappa,\kappa',\mu)$ reduce to the following simple product of Clebsch-Gordan coefficients:

$$G(\kappa,\kappa',\mu)=C(lj\tfrac{1}{2},\mu-s,s)C(lj'\tfrac{1}{2};\mu-s,s)-C(lj\tfrac{1}{2};\mu+s,-s)C(lj'\tfrac{1}{2};\mu+s,-s)\ , \tag{5}$$

$$-j\le\mu\le j\ . \tag{6}$$

Rather than solving a coupled set of Volterra like equations, the general solutions for $r\le R_s$ (R_s is the muffin-tin radius) are obtained through a matching at $r=R_s$ with the solutions of Eqs. (1) and (2) for $V_{\text{eff}}(r)=B_{\text{eff}}(r)=0$. The matching can be formulated in terms of a single-site t matrix whose elements are given as follows:[2]

$$t_{\kappa_1\mu,\kappa_1\mu}(E)=\frac{1}{ip}\frac{\Delta^{(1)}j_{l_1}(pR_s)-\dfrac{ip}{p_0+1}S_{\kappa_1}j_{\bar{l}_1}(pR_s)}{\Delta^{(1)}h^+_{l_1}(pR_s)-\dfrac{ip}{p_0+1}S_{\kappa_1}h^+_{\bar{l}_1}(pR_s)}\ , \tag{7}$$

$$t_{\kappa_1\mu,\kappa_2\mu}(E)=\frac{j_{l_1}(pR_s)-ipt_{\kappa_1\mu,\kappa_1\mu}(E)h^+_{l_1}(pR_s)}{F^{(1)}_1\bar{g}_{\kappa_1\mu,1}(E,R_s)+F^{(1)}_2\bar{g}_{\kappa_1\mu,2}(E,R_s)}\ , \tag{8}$$

$$\Delta^{(1)}=\frac{F^{(1)}_1 i\bar{f}_{\kappa_1\mu,1}(E,R_s)+F^{(1)}_2 i\bar{f}_{\kappa_1\mu,2}(E,R_s)}{F^{(1)}_1\bar{g}_{\kappa_1\mu,1}(E,R_s)+F^{(1)}_2\bar{g}_{\kappa_1\mu,2}(E,R_s)}\ , \tag{9}$$

$$F^{(1)}_1=-ip\frac{\left[\dfrac{ip}{p_0+1}\right]S_{\kappa_2}h^+_{l_2}(pR_s)-a_{\kappa_2\mu,2}h^+_{l_2}(pR_s)}{i\bar{f}_{\kappa_2\mu,1}(E,R_s)-a_{\kappa_2\mu,2}\bar{g}_{\kappa_2\mu,1}(E,R_s)}\ , \tag{10}$$

$$F^{(1)}_2=-ip\frac{\left[\dfrac{ip}{p_0+1}\right]S_{\kappa_2}h^+_{\bar{l}_2}(pR_s)-a_{\kappa_2\mu,1}h^+_{l_2}(pR_s)}{i\bar{f}_{\kappa_2\mu,1}(E,R_s)-a_{\kappa_2\mu,1}\bar{g}_{\kappa_2\mu,2}(E,R_s)}\ , \tag{11}$$

$$a_{\kappa\mu,\nu}=\frac{i\bar{f}_{\kappa\mu,\nu}(E,R_s)}{\bar{g}_{\kappa\mu,\nu}(E,R_s)}\ , \tag{12}$$

$$p_0=E,\quad E^2=p^2+1,\quad S_\kappa=\kappa/|\kappa|\ . \tag{13}$$

In Eqs. (9)–(12) the $\bar{f}_{\kappa\mu,\nu}(E,r)$ and $\bar{g}_{\kappa\mu,\nu}(E,r)$ are elements of a 4 vector of radial solutions of Eqs. (1) and (2) with the following boundary conditions at the origin:

$$(\bar{g}_{\kappa_1\mu,\nu},i\bar{f}_{\kappa_1\mu,\nu},\bar{g}_{\kappa_2\mu,\nu},i\bar{f}_{\kappa_2\mu,\nu})=\begin{cases}(1,P(\kappa_1),0,0), & \nu=1\\ (0,0,1,P(K_2)), & \nu=2\ ,\end{cases} \tag{14}$$

$$P(\kappa_i)=\frac{\kappa_i+S(\kappa_i)}{2Z/c}\ , \tag{15}$$

$$S(\kappa_i)=[\kappa_i^2-(2Z/c)^2]^{1/2}\ . \tag{16}$$

For the calculation of $t_{\kappa_2\mu,\kappa_1\mu}$ and $t_{\kappa_2\mu,\kappa_2\mu}$ the superscript (1) in Eqs. (9)–(11) are replaced by superscript (2), i.e., the case $\nu=2$ in Eq. (14) applies.

From the single-site t matrix $t_{QQ'}(E)$ the partial scattering amplitudes $f_{QQ'}(E)$ and the single-site S matrix $S_{QQ'}(E)$ are obtained

$$f_{QQ'}(E)=-\sqrt{E}\,t_{QQ'}(E)\ , \tag{17}$$

$$S_{QQ'}(E)=\delta_{QQ'}-2if_{QQ'}(E)\ . \tag{18}$$

The single-site t matrix has the structure shown in Fig. 1.

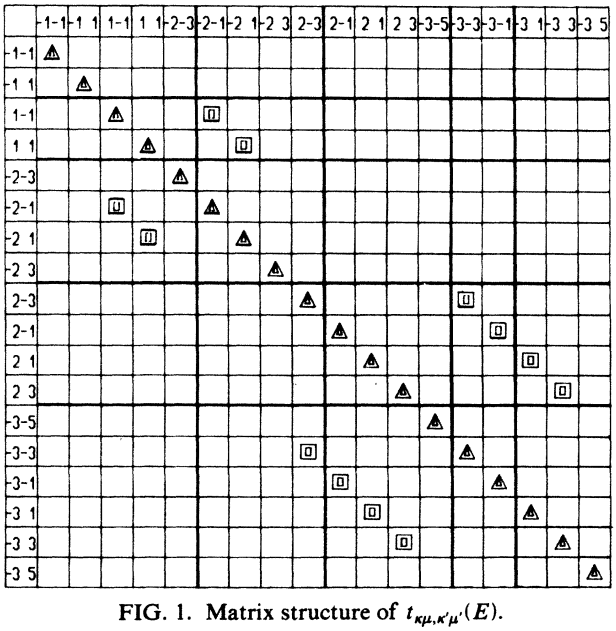

FIG. 1. Matrix structure of $t_{\kappa\mu,\kappa'\mu'}(E)$.

For a particular value of l and μ, the t matrix can be described in terms of at most three partial scattering amplitudes. For $B_{\text{eff}}=0$ and for resonant angular momentum channels, the scattering amplitudes change counterclockwise along the unitary circle. At the resonant energy, the energy at which the phase shift passes through $\pi/2$, the scattering amplitude passes the imaginary axis. For $B_{\text{eff}}\neq 0$ the scattering amplitude in general no longer moves along the unitary circle. The scattering in a particular channel is said to be absorptive (emissive) if the scattering amplitude is inside (outside) the unitary circle. In the case of absorptive scattering one still can talk rather safely about a "predominant" resonant energy if the scattering amplitude crosses the imaginary axis well above 0.5. Of course, one can also diagonalize the single-site S matrix and define two corresponding complex phase shifts (see also the discussion by Strange *et al.*[2]). In the following section resonant energies for a particular scattering channel $Q=(\kappa\mu)$ shall be defined by the energy at which the diagonal scattering amplitude $f_{QQ}(E)$ crosses the imaginary axis above 0.5.

As already pointed out by Strange *et al.*[2] and Feder *et al.*[3] the single-site t matrix can be used for relativistic spin-polarized multiple scattering. From the scattering path operator (cf. the discussion by Staunton *et al.*[6] and Weinberger *et al.*[7]) the nonsite diagonal scattering path operator corresponding to the sites $\mathbf{R}_i$ and $\mathbf{R}_j$ for simple lattices is given by

$$\underline{\tau}^{ij}(E)=\frac{1}{\Omega_{\text{BZ}}}\int[\underline{t}^{-1}(E)-\underline{G}(E,\mathbf{k})]^{-1}e^{i\mathbf{k}\cdot(\mathbf{R}_i-\mathbf{R}_j)}d\mathbf{k}$$
$$=\frac{1}{\Omega_{\text{BZ}}}\int\underline{\tau}(E,\mathbf{k})e^{i\mathbf{k}\cdot(\mathbf{R}_i-\mathbf{R}_j)}d\mathbf{k} \tag{19}$$

where $\underline{t}(E)$ is the single-site t matrix Eqs. (7) and (8) and $\underline{G}(E,\mathbf{k})$ are the relativistic KKR-structure constants. The poles of $\underline{\tau}(E,\mathbf{k})$ correspond to energies for which the determinant of the KKR matrix vanishes:

$$\det[\underline{\tau}(E,\mathbf{k})^{-1}]=\det[\underline{t}^{-1}(E)-\underline{G}(E,\mathbf{k})]=0\ . \tag{20}$$

Energies at which Eq. (20) is fulfilled along a particular ray in the Brillouin zone constitute the spin-polarized relativistic energy bands.

According to Rose[8] the relativistic Green's function is written as a 2×2 matrix in spin space

$$\underline{G}(E,\mathbf{r},\mathbf{r}')=\begin{bmatrix}G_{11}(E,\mathbf{r},\mathbf{r}') & G_{12}(E,\mathbf{r},\mathbf{r}')\\ G_{21}(E,\mathbf{r}\mathbf{r}') & G_{22}(E,\mathbf{r},\mathbf{r}')\end{bmatrix}. \tag{21}$$

In terms of the scattering path operator the relativistic Green's function is given by[9–11]

$$\underline{G}(E,\mathbf{r},\mathbf{r}')=\sum_{l,\mu}[\underline{Z}^{i}_{l,\mu}(E,\mathbf{r}_i)\underline{\tau}^{ij}_{l,\mu}(E)\underline{Z}^{j}_{l,\mu}(E,\mathbf{r}'_j)$$
$$-\delta_{ij}\underline{Z}^{i}_{l,\mu}(E,\mathbf{r}_i)\underline{J}^{j}_{l,\mu}(E,\mathbf{r}'_j)]\ . \tag{22}$$

In Eq. (22) $\underline{Z}^{i}_{l,\mu}(E,\mathbf{r}_i)$, $\underline{J}^{i}_{l,\mu}(E,\mathbf{r}_i)$, and $\underline{\tau}^{ij}_{l,\mu}(E)$ are 2×2 matrices:

$$\underline{Z}^{i}_{l,\mu}(E,\mathbf{r}_i)=\begin{bmatrix}Z^{i,\nu=1}_{\kappa\mu}(E,\mathbf{r}_i) & Z^{i,\nu=1}_{\kappa'\mu}(E,\mathbf{r}_i)\\ Z^{i,\nu=2}_{\kappa\mu}(E,\mathbf{r}_i) & Z^{i,\nu=2}_{\kappa'\mu}(E,\mathbf{r}_i)\end{bmatrix}, \tag{23}$$

$$\underline{J}^{i}_{l,\mu}(E,\mathbf{r}_i)=\begin{bmatrix}J^{i,\nu=1}_{\kappa\mu}(E,\mathbf{r}_i) & J^{i,\nu=1}_{\kappa'\mu}(E,\mathbf{r}_i)\\ J^{i,\nu=2}_{\kappa\mu}(E,\mathbf{r}_i) & J^{i,\nu=2}_{\kappa'\mu}(E,\mathbf{r}_i)\end{bmatrix}, \tag{24}$$

$$\underline{\tau}^{ij}_{l,\mu}(E)=\begin{bmatrix}\tau^{ij}_{\kappa\mu,\kappa\mu}(E) & \tau^{ij}_{\kappa\mu,\kappa'\mu}(E)\\ \tau^{ij}_{\kappa'\mu,\kappa\mu}(E) & \tau^{ij}_{\kappa'\mu,\kappa'\mu}(E)\end{bmatrix}. \tag{25}$$

The functions $Z^{i,\nu}_{\kappa\mu}(E,\mathbf{r}_i)$ are normalized according to Eq. (2.11) of Strange *et al.*:[2]

$$Z^{i,\nu}_{\kappa\mu}(E,\mathbf{r}_i)=\begin{bmatrix}g^{i,\nu}_{\kappa\mu}(E,r_i)\,|\,\kappa\mu\rangle\\ if^{i,\nu}_{\kappa\mu}(E,r_i)\,|\,-\kappa\mu\rangle\end{bmatrix}, \tag{26}$$

where the $|\,\kappa\mu\rangle$ are the spin spherical harmonics, while the functions

$$J^{i,\nu}_{\kappa\mu}(E,\mathbf{r}_i)=\begin{bmatrix}\tilde{g}^{i,\nu}_{\kappa\mu}(E,r_i)\,|\,\kappa\mu\rangle\\ i\tilde{f}^{i,\nu}_{\kappa\mu}(E,r_i)\,|\,-\kappa\mu\rangle\end{bmatrix} \tag{27}$$

are normalized such that at the muffin-tin radius ($r_i=R_s$)

$$[J^{i,\nu}_{\kappa\mu}(E,r_i),J^{i,\nu}_{\kappa'\mu}(E,r_i)]$$
$$=\begin{cases}\left[j_l(Er_i),\dfrac{ipS_\kappa}{p_0+1}j_{\bar{l}}(Er_i),0,0\right], & \nu=1\\ \left[0,0,j_{l'}(Er_i),\dfrac{ipS_\kappa}{p_0+1}j_{\bar{l}'}(Er_i)\right], & \nu=2\ .\end{cases} \tag{28}$$

The indices κ and κ' have the following two values:

$$\kappa=-l-1,\ l\ ,$$
$$\kappa'=l,\ -l-1\ . \tag{29}$$

In terms of the site-diagonal Green's function the first-order density matrix is given as

$$n(E,\mathbf{r})=-\pi^{-1}\,\text{Im}\,\text{Tr}\,G(E,\mathbf{r},\mathbf{r})$$
$$=-\pi^{-1}\,\text{Im}\sum_{l,\mu}\sum_{\nu=1,2}\sum_{\kappa=-l-1,\,l}\sum_{\kappa'=l,\,-l-1}[Z^{i,\nu}_{\kappa\mu}(E,\mathbf{r}_i)\tau^{ii}_{\kappa\mu,\kappa'\mu}(E)Z^{i,\nu}_{\kappa'\mu}(E,\mathbf{r}_i)-Z^{i,\nu}_{\kappa\mu}(E,\mathbf{r}_i)J^{i,\nu}_{\kappa'\mu}(E,\mathbf{r}_i)]\ , \tag{30}$$

where Tr denotes the trace over the spinors. The density of states is therefore given by

$$n(E)=\int_{\Omega_i}n(E,\mathbf{r})d\mathbf{r}=-\pi^{-1}\,\text{Im}\sum_{l,\mu}\sum_{\nu=1,2}\sum_{\substack{\kappa=-l-1,\,l\\ \kappa'=l,\,-l-1}}R^{i,\nu}_{\kappa\mu,\kappa'\mu}(E)\tau^{ii}_{\kappa\mu,\kappa'\mu}(E)\ , \tag{31}$$

where

$$R^{i,\nu}_{\kappa\mu,\kappa'\mu}(E)=\int_{\Omega_i} Z^{i,\nu}_{\kappa\mu}(E,\mathbf{r}_i)Z^{i,\nu}_{\kappa'\mu}(E,\mathbf{r}_i)d\mathbf{r}_i \ , \tag{32}$$

and Ω_i denotes the volume of the unit cell.

III. COMPUTATIONAL DETAILS

This first attempt to include spin-polarization in a fully relativistic treatment for the t matrices and band states was performed by a non-self-consistent procedure. Since Eqs. (1) and (2) require as input a V_{eff} and B_{eff}, and since the calculations are to be performed for a solid, a V_{eff} and B_{eff} that was constructed from a solid-state calculation seemed preferable to using atomic potentials. With that in mind, self-consistent scalar relativistic spin-polarized linear muffin-tin orbital (LMTO) calculations were performed for Ce and Pu at lattice spacings corresponding to Wigner-Seitz radii of 3.82 and 3.42, respectively (both systems are spin-polarized at these spacings). From these calculations, B_{eff} ($B_{\text{ext}}=0$) was constructed by taking the difference of the muffin-tin spin-up and spin-down densities and the paramagnetic effective potential V_{eff} by averaging the corresponding spin-up and spin-down potentials. The value of $V_{\text{eff}}(r)$ at the muffin-tin radius is considered to be the constant potential outside the muffin-tin. Because the main purpose of the present calculations is to illustrate the effects of the coupling between spin-orbit and spin-polarization and is not self-consistent, this rather crude procedure seemed reasonable. The single-site results are obtained by solving Eqs. (7) and (8) using Eqs. (9)—(16). The energy-band results are obtained by solving Eq. (20) which uses Eqs. (21)—(28) for the above potential.

IV. RESULTS

A. Single-site scattering

In Figs. 2—5 we show the resonant energies as a function of the fictitious external magnetic field B_{ext} for both Ce and Pu. In a solid the resonant energies, defined as the energies at which the diagonal scattering amplitude $f_{QQ}(E)$ crosses the imaginary axis above 0.5, are the closest analogy to energy eigenvalues in atoms. As such they can be used to indicate the way that spin-orbit and spin-polarization interactions couple and split the electronic states. The external field is fictitious in the sense that it only couples to the spin degrees of freedom and not to the orbital currents. It enters through Eq. (3) as an energy $\mu_B B_{\text{ext}}$ (where μ_B is a Bohr magneton represented by $e\hbar/2mc$); its value is given in Ry energy units. Also, since the range of variation in Figs. 2—5 is typically at least 3 orders of magnitude larger than most laboratory magnets can achieve, it is probably best to think of it as a variation in the strength of the spin-polarization potential, cf. Eq. (3).

In this paper we have chosen B_{ext} to be of opposite sign from $\delta E_{\text{xc}}/\delta \mathbf{m}(r)$. When B_{ext} is of the same order of magnitude as the spin-polarization effective field, the two contributions cancel each other ($B_{\text{eff}}\approx 0$) and the present theory reduces to the normal nonmagnetic Dirac fully relativistic theory. For the resonant energies this is seen quite clearly in Fig. 2(b) for B_{ext} near 0.02 Ry, where the resonant energies cluster near the degenerate nonmagnetic spin-orbit split ($f^{5/2}$ and $f^{7/2}$) resonant energies. Increasing or decreasing B_{ext} then is a way of examining how the spin-orbit and spin-polarization effects couple and interact with each other as the strength of the effective spin-polarization is varied relative to the size of the spin-orbit splitting. In Fig. 2(b) the pattern and size of the energy splitting is symmetrical above and below 0.02 Ry and is equivalent to simply changing the sign of B_{eff}. This is also shown by the way the pattern of μ quantum numbers invert relative to each other at either end of the figure, when the effective spin-polarization term is largest. At these extremes the pattern of resonant energies resembles a normal spin-polarized calculation, with a cluster of 7 spin-up and 7 spin-down energies, which are then in turn additionally split by the spin-orbit coupling into almost Zeeman-type patterns. It is interesting to follow how one of the resonant energies from the $f^{7/2}$ level is pulled off to achieve the 7+7 pattern as B_{ext} is varied away from the position when $B_{\text{eff}}\approx 0$. These patterns were also seen in the spin-polarized relativistic calculations of Strange *et al.*[2] for the Pt d resonant energies and by those of Cortona *et al.*[4] for the rare-earth $4f$ atomic eigenvalues.

The qualitative pattern of the resonant energies holds equally well for both d and f electrons. Quantitatively, the relative size of the spin-orbit splitting and the effective spin-polarized potential will vary from system to system and between d and f electrons for the same system. In Ce, for example, the d resonance patterns overlap [Fig. 2(a)], whereas the f resonance patterns [Fig. 2(b)] are well separated and easier to follow (as are also the Pt d resonance patterns calculated by Strange *et al.*[2] and the Pu f resonance energies in Fig. 4). Physically, the reason for breaking the degeneracy of the resonant energies (or atomic eigenvalues) is because the spin-orbit coupling breaks the rotational symmetry in the presence of the spin-polarization, unlike the nonrelativistic case where the spin and orbital degrees of freedom are completely decoupled.

In Fig. 2(a) are shown the d resonant energies for Ce. At the left of the figure are the normal degenerate relativistic $d^{3/2}$ and $d^{5/2}$ resonant energies, split by a spin-orbit splitting of about 0.03 Ry. The pattern of resonant energies at fields of 0.01 and 0.02 Ry are nearly identical, but with the μ labels inverted with respect to each other. Hence, the effective field B_{ext} that is needed to compensate the spin-polarized potential is of the order of 0.015 Ry. The spin-orbit splitting is approximately double this value. The strong overlap in the pattern of resonant energies is very different from all the other calculations in the paper [see Figs. 2(b) and 4] and the Pt d results of Strange *et al.*[2]

In Fig. 2(b) we show the corresponding Ce resonant energies for the f electrons. In this case the spin-orbit splitting ($\sim$0.02 Ry) is almost the same as the effective spin-polarization field (note the pattern of energies for $B_{\text{ext}}\sim 0.02$ Ry). Here the classic pattern that we have discussed above emerges. One of the $f^{7/2}$ states is split off and added to the $f^{5/2}$ cluster to form two clusters of 7 states. The center of gravity of the upper cluster moves to

higher energies for larger B_{ext} while the lower cluster moves to lower energies. For very large B_{ext} the states within each cluster remain split by about the same amount while the separation between the center of gravity of the two clusters increases proportional to B_{ext}.

In Fig. 3 we plot each of the states more explicitly as a function of B_{ext}. All of the states, except for two, are clearly symmetrical about B_{ext} of 0.022 Ry. The $\mu=\frac{7}{2}$ and $-\frac{7}{2}$ states are different because it is these states that are pulled off from the $j=\frac{7}{2}$ states and added to the $j=\frac{5}{2}$ states to even up the number of states of the lower and upper clusters at 7 states each. At large B_{ext} the plots seem approximately linear in B_{ext} and equal for all μ. The slope is probably a measure of the rate of separation

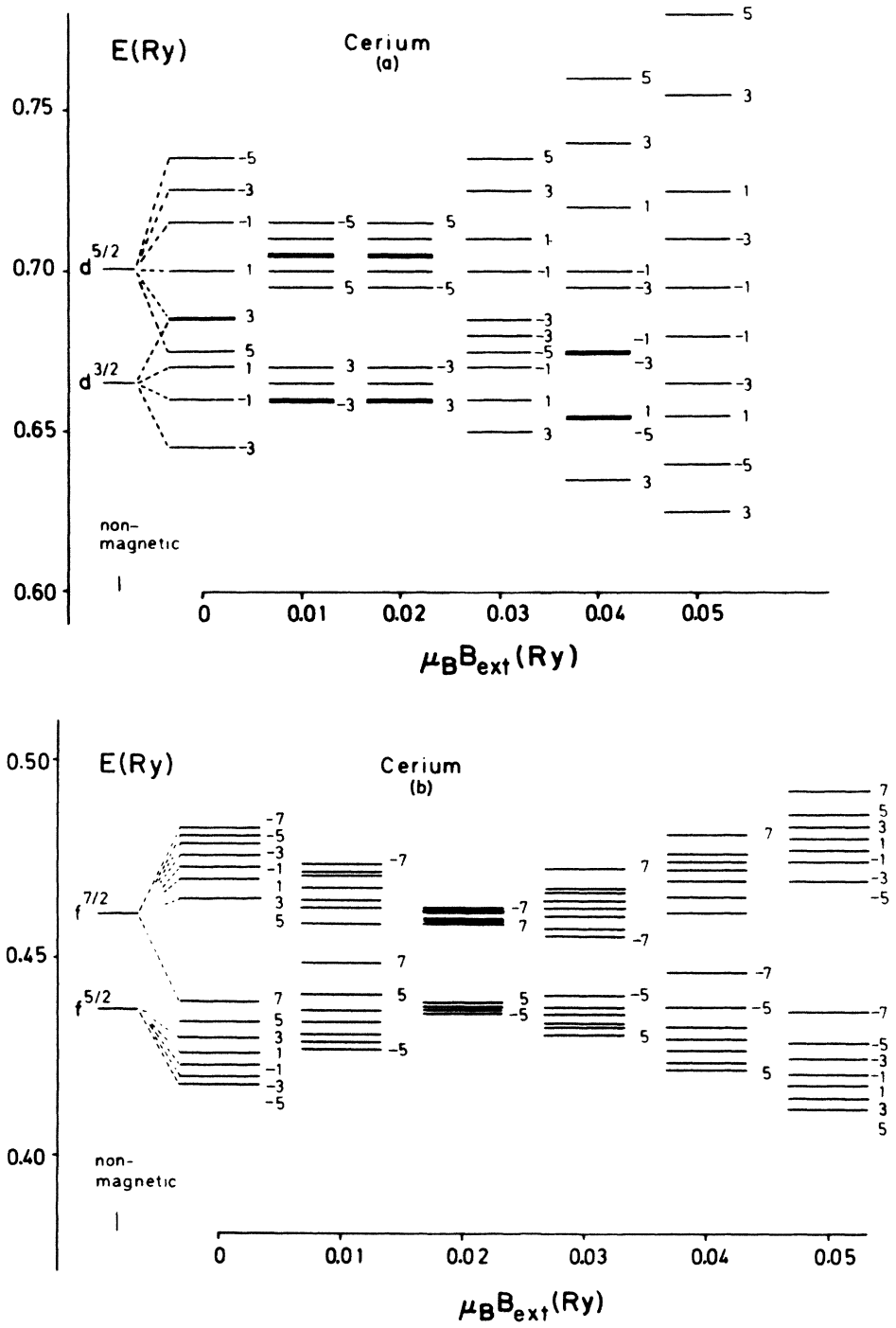

FIG. 2. (a) Resonant energies for the diagonal d-type scattering amplitudes ($\kappa=\kappa'=-3,2$) in Ce. The quantum number μ is shown as 2μ. (b) Resonant energies for the diagonal f-type scattering amplitudes ($\kappa=\kappa'=-4,3$) in Ce. The quantum number μ is shown as 2μ.

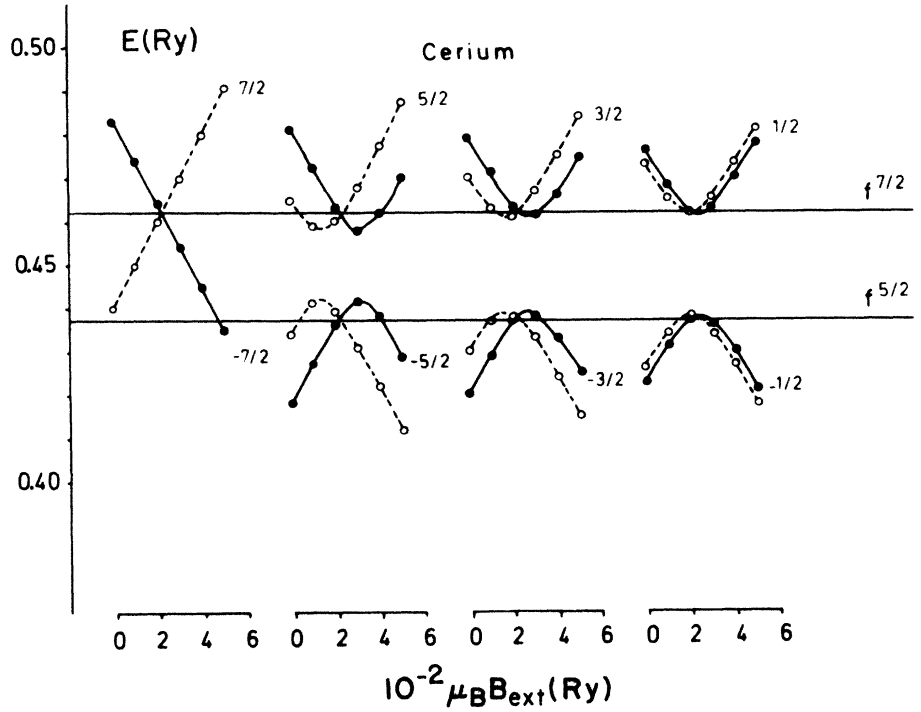

FIG. 3. Variation of the resonant energies for the diagonal f-type scattering amplitudes in Ce with respect to the external magnetic field.

of the center of gravity of the clusters. Calculations for much larger B_{ext} are needed to test this quantitatively.

In Fig. 4 we show the f-electron resonant energies of Pu as a function of B_{ext}. The patterns are similar qualitatively to those of Ce. In this case the spin-orbit splitting ($\sim$0.1 Ry) is also about the same as the spin-polarization field ($\sim$0.12 Ry), and both are about an order of magnitude larger than the corresponding quantities for Ce. In Fig. 5 we again show explicitly how the $\mu=\pm 7/2$ states are pulled away from the $f^{7/2}$ states to form the two clus-

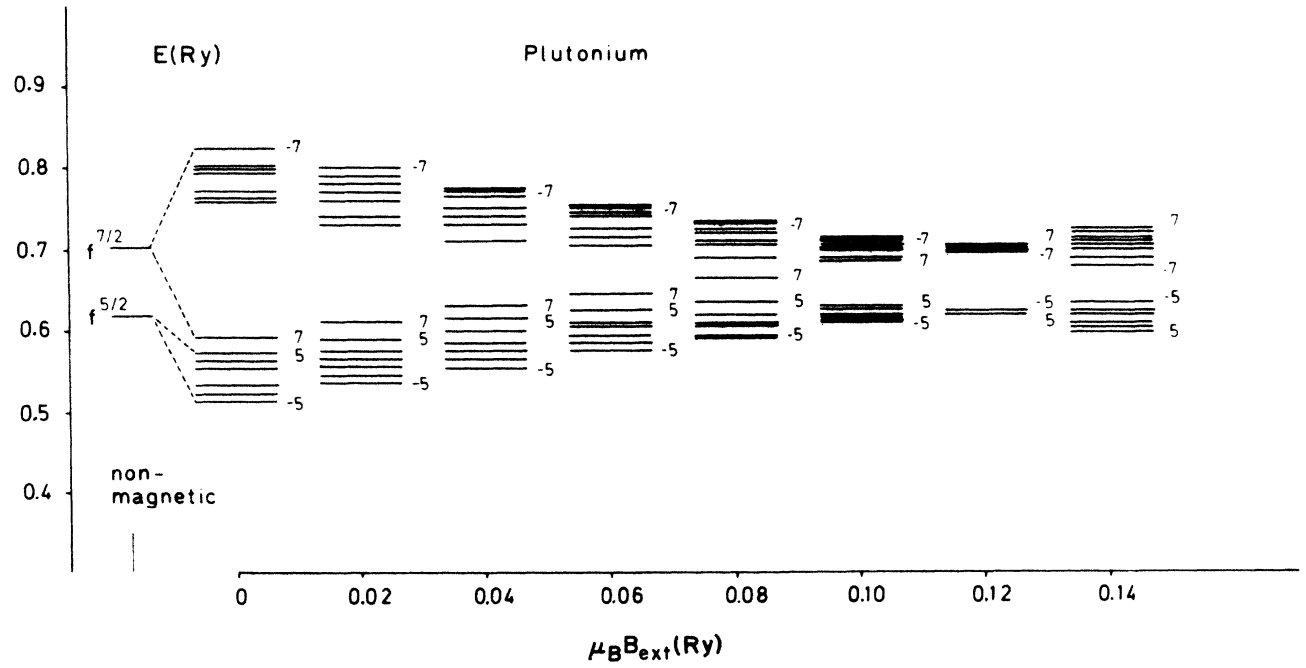

FIG. 4. Resonant energies for the diagonal f-type scattering amplitudes ($\kappa=\kappa'=-4,3$) in Pu.

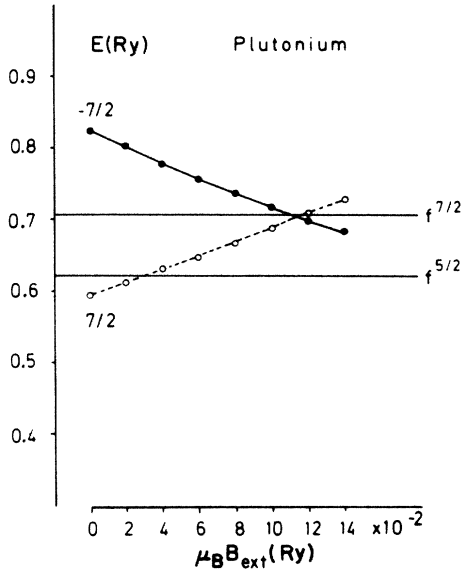

FIG. 5. Variation of the resonant energy for the $\mu=\pm\frac{7}{2}$ f-type scattering amplitude in Pu with respect to the external magnetic field.

ters of 7 states. For Pu we have not shown the d resonances. They are so weak that the nonmagnetic $d^{3/2}$ and $d^{3/2}$ phase shifts never reach $\pi/2$ within the energy range 0—2 Ry.

In Fig. 6 the f-type scattering amplitudes for Ce corresponding to $\mu=\pm\frac{5}{2}$ are shown as a typical example at zero external field scattering. In particular, Fig. 6 suggests that the concept of resonant energies can at best provide only a somewhat qualitative picture of single-site scattering. Using the diagonalized form of the S matrix [Eq. (18)] as discussed by Strange *et al.*,[2] however, the corresponding resonant energies are only marginally different from the ones shown in Figs. 2 and 3.

In Fig. 7 the variation of the $\mu=\frac{3}{2}$ (for Ce) off-diagonal f-type scattering amplitude ($\kappa=-4$, $\kappa'=3$) with respect to the external field is shown. For B_{ext} of 0.022 Ry the scattering is completely elastic, i.e., the contour of the off-diagonal scattering amplitude is reduced to a limiting circle. As the external magnetic field becomes larger than the internal magnetic field, the off-diagonal scattering amplitude starts growing again. The d-type scattering amplitudes ($\kappa=\kappa'=-3,2$) are almost elastic. The d-type off-diagonal scattering amplitudes ($\kappa=-3$, $\kappa'=2$) are shown in Fig. 8 for $\mu=\frac{3}{2}$ for B_{ext} of 0.0, 0.01, 0.02, and 0.03 Ry.

Since scattering amplitudes are implicit functions of the energy parameter E, for Pu the f-type scattering amplitudes ($\kappa=\kappa'=-4,3$) and the f-type off-diagonal scattering amplitudes are very similar in shape to the corresponding amplitudes in Ce. Separate figures for the f-type scattering in Pu are therefore not shown. As already mentioned, however, in the case of Pu much bigger external magnetic fields are needed in order to compensate the internal splitting.

B. Relativistic spin-polarized energy bands for Ce

Using the single-site t matrices discussed in Sec. IV A for Ce relativistic spin-polarized energy bands along (100) and (111) of the fcc Brillouin zone are calculated in the

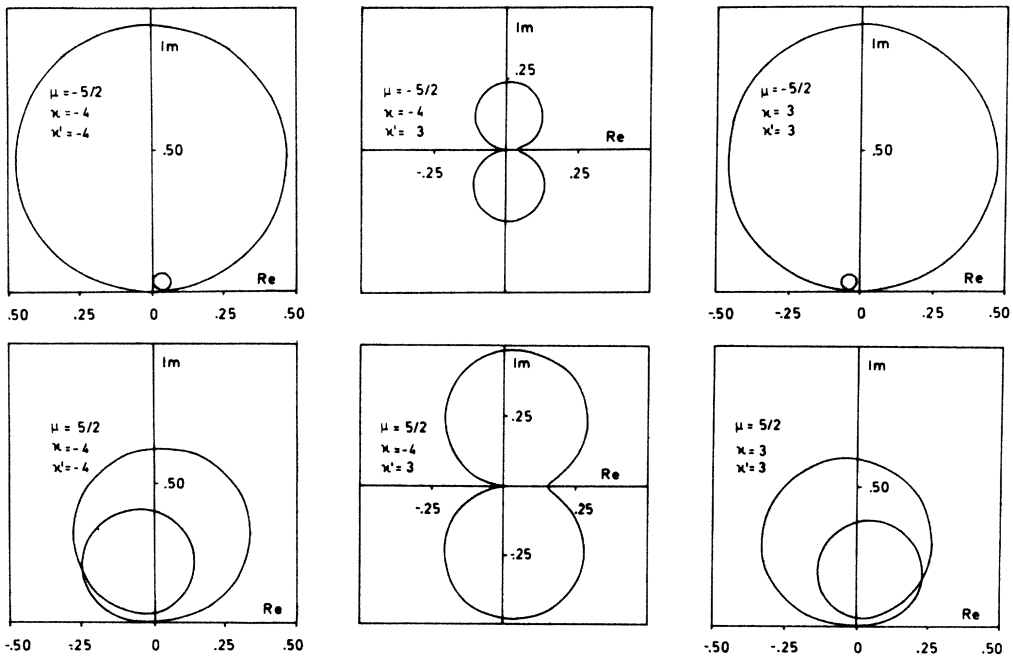

FIG. 6. Diagonal f-type scattering amplitudes in Ce for $\mu=\pm\frac{5}{2}$ in the absence of an external magnetic field. The top row corresponds to $\mu=-\frac{5}{2}$, the bottom row to $\mu=\frac{5}{2}$. In the left (right) column κ and κ' are -4 (3).

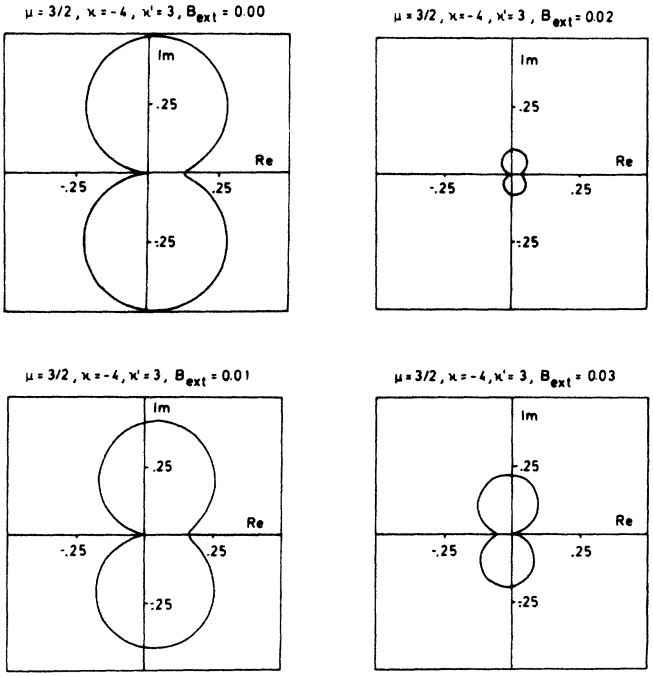

FIG. 7. Variation of the $\mu=\frac{3}{2}$ f-type off-diagonal scattering amplitude ($\kappa=-4$, $\kappa'=3$) in Ce with respect to the applied external magnetic field.

presence of only the internal spin-polarized field ($B_{\text{ext}}=0$). These energy bands are shown on the right-hand side of Figs. 9 and 10 together with their nonmagnetic counterparts on the left-hand side. In both figures one clearly can see the *sd* band penetrating the complex of f-type bands (Γ^- states) from below. Along (100) also a typical d-type band (Γ^+) coming from above penetrates the f bands. The dispersion of the "nonmagnetic" and the "magnetic" bands is similar for all cases with similar compatibility relations such as the *sd* band (starting at Γ_6^+ and ending at X_6^+ or L_6^+ in the nonmagnetic case) or the d-type band starting at the bottom Γ_7^- state. In the vicinity of the f bands, however, different compatibility relations pertain in the magnetic case. In general, the spin polarization removes all remaining degeneracy from the fully relativistic bands.

At the bottom of the s band, at Γ, a very special case can be discussed. Since Γ_6^+ only has s symmetry, i.e., the irreducible basis functions of Γ_6^+ are $(\kappa,\mu)=(-1,-\frac{1}{2})$ and $(-1,-\frac{1}{2})$, and since the $(-1,-\frac{1}{2})$ and $(-1,\frac{1}{2})$ channels cannot mix [see also Eqs. (1) and (5)], the splitting of Γ_6^+ into two magnetic states is completely analogous to a nonrelativistic spin polarization. In Fig. 11 the two states are shown as a function of the external field B_{ext}, i.e., are shown with decreasing internal field. As can be seen in this figure the splitting due to $B_{\text{eff}}(r)$ is completely symmetric. For vanishing $B_{\text{eff}}(r)$ these two states degenerate into Γ_6^+.

For other states at Γ the situation is much more complex not only because in the magnetic case the κ values belonging to one l mix, but also because for irreducible representations other than Γ_6^+ the irreducible representations show combinations of different μ values. The Γ_8^- is the most interesting case and has a very complex set of f-type irreducible basis functions (Onodera and Okazaki,[12] Dirl *et al.*[13]). An assignment of the relativistic spin-polarized bands with respect to the relativistic, nonmagnetic bands is therefore in general not directly possible. Even for the

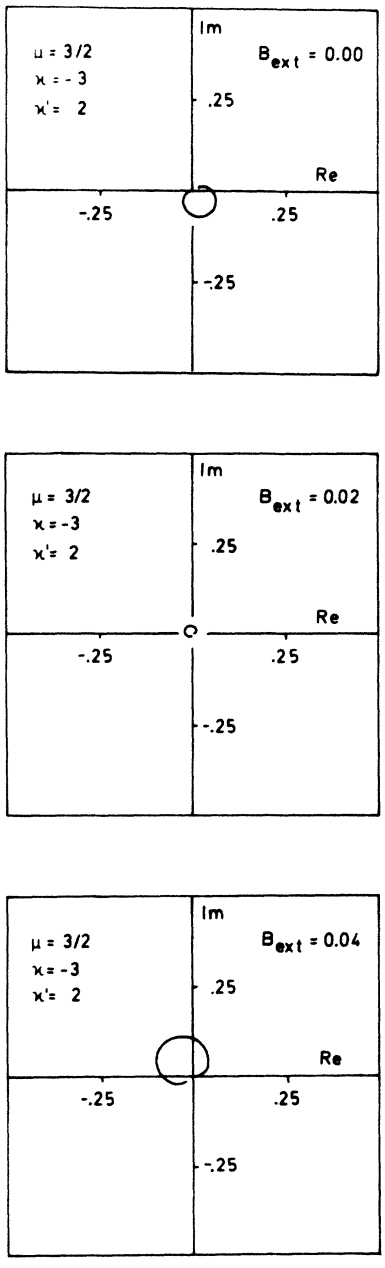

FIG. 8. Variation of the $\mu=\frac{3}{2}$ d-type off-diagonal scattering amplitude ($\kappa=-3$, $\kappa'=2$) in Ce with respect to the applied external magnetic field.

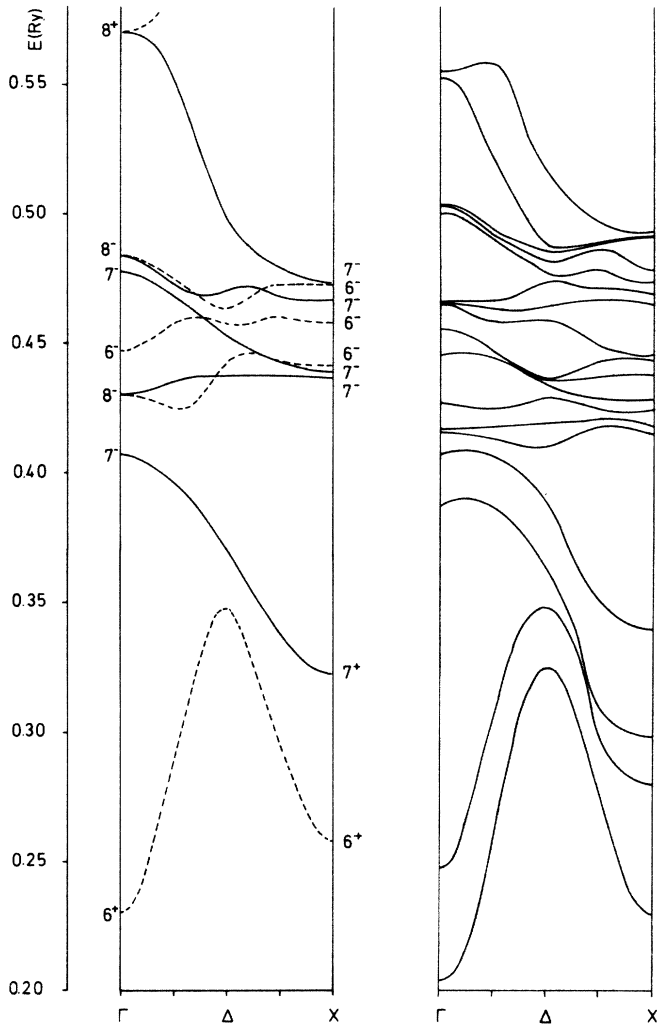

FIG. 9. Energy bands along ⟨100⟩ for Ce. The left-hand side of the figure shows the nonmagnetic, relativistic bands, the right-hand side the relativistic spin-polarized bands ($B_{ext}=0.0\times e\hbar/2mc$, Ry).

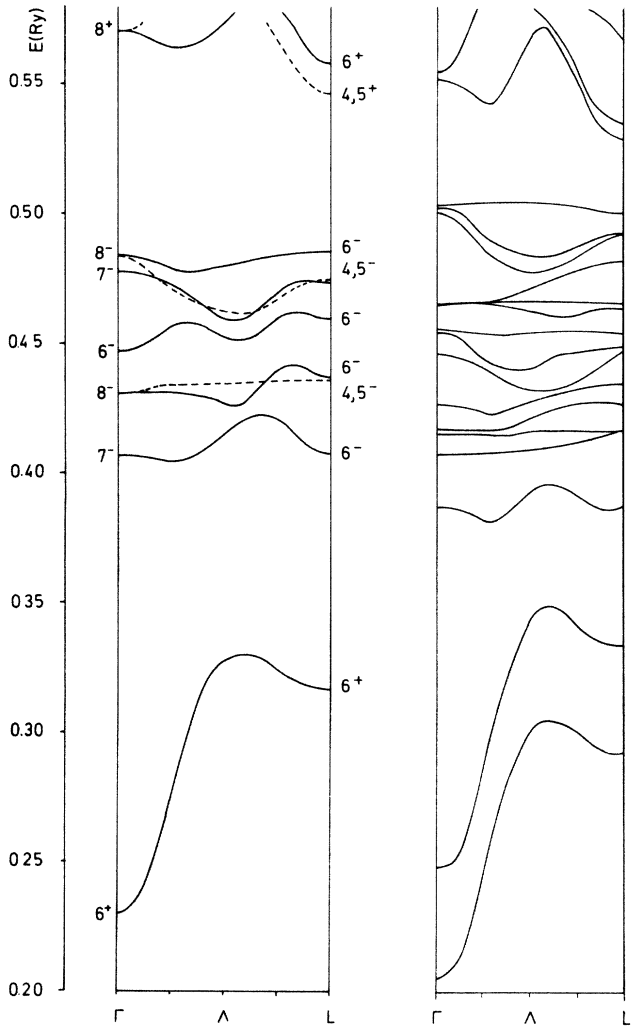

FIG. 10. Energy bands along ⟨111⟩ for Ce. The left-hand side of the figure shows the nonmagnetic, relativistic bands, the right-hand side the relativistic spin-polarized bands ($B_{ext}=0.0\times e\hbar/2mc$, Ry).

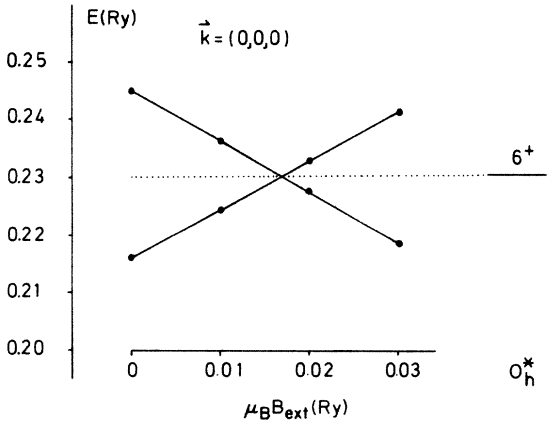

FIG. 11. Spin-polarization effects for the bottom of the s band in Ce.

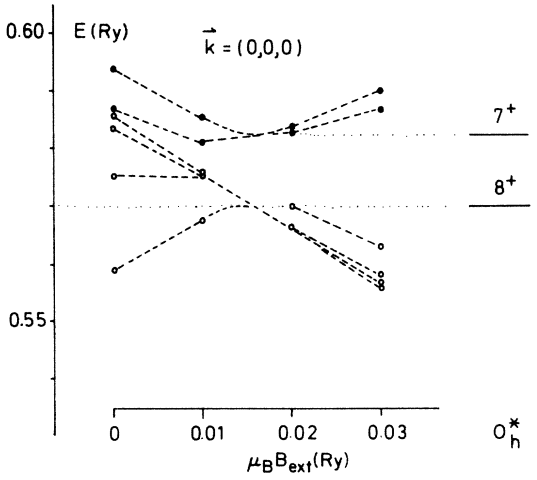

FIG. 12. Spin-polarization effects for the Γ_7^+ and the lower Γ_8^+ state in Ce.

relatively simple case of d-type states at Γ the situation is somewhat complex. Figure 12 shows the splitting of the Γ_7^+ and the lower Γ_8^+ state in Ce. Again one can see that for vanishing $B_{\text{eff}}(r)$ these states do degenerate into Γ_7^+ (2 states) and Γ_8^+ (4 states); however, the collapse of the splitting is not as straightforward as for Γ_6^+ (Fig. 11).

V. CONCLUSIONS

Whether resonant energies or the energy bands themselves are examined, the main effect of spin polarization on the fully relativistic electronic states is to split all remaining degeneracy. The coupling between all the different states is highly complex and the resulting pattern of energies can be quite complicated and difficult to understand (for example, the Ce d overlapping resonant energies and the Ce $4f$ band structure results). In some cases, such as the Ce and Pu f and Pu d resonant energies, the resulting pattern of energies for large internal spin-polarization fields resembles two sets of an equal number of states that look like spin-up and spin-down states that are in turn split by the spin-orbit effects. In terms of the energy patterns of these states, one cannot distinguish any qualitative differences between d and f electrons. The Ce d case is unlike all the above in that the present calculations seem to indicate that the pattern of resonant energies will overlap for values of B_{ext} larger than the spin-polarized splitting.

While the present results give one some feeling for what to expect from these types of calculations, the next step is to calculate the electronic structure of systems like Ce and Pu self-consistently with respect to the charge density and the magnetization density. By using a fully relativistic KKR-type approach based on complex energies this is not an unsurmountable problem. In addition it should be noted that within the framework of the CPA-KKR method spin-polarized relativistic scattering can also be applied to substitutionally disordered systems. For the time being, the present paper quite clearly shows what kind of effects can be expected in a full scale spin-polarized relativistic calculation of the electronic structure of f-electron systems.

A final comment should be made about the symmetry breaking created by the relativistic spin-polarized calculations as they have been developed here and by previous workers.[1-4] As has been shown, the coupling between the spin orbit and spin polarization leads to the breaking of rotational symmetry around a given site. For isolated atoms or ions with unfilled shells one does not have spherical symmetry, but the calculations are performed for the configuration average in a spherical potential so it is interesting that no degeneracy is left. Whether or not an orbital contribution to the magnetization in the isolated ion case would restore some of the degeneracy is unknown. Also, how one would include such a contribution in the solid state case is not clear.

ACKNOWLEDGMENTS

One of us (P.W.) wants to acknowledge a grant by the Austrian National Bank (Project 2301). We also thank Paul Strange, John Wilkins, and Seb Doniach for several interesting discussions on this topic.

[1]A. H. MacDonald and S. H. Vosko, J. Phys. C **12**, 2977 (1979); A. K. Rajagopal, *ibid.* **11**, L943 (1978); M. V. Ramana and A. K. Rajagopal, Adv. Chem. Phys. **LIV**, 231 (1980); A. H. MacDonald, J. Phys. C **16**, 3869 (1983); BuXing Xu, A. K. Rajagopal, and M. V. Ramana, *ibid.* **17**, 1339 (1984).

[2]P. Strange, J. Staunton, and B. L. Gyorffy, J. Phys. C **17**, 3355 (1984).

[3]R. Feder, F. Rosicky, and B. Ackermann, Z. Phys. B **52**, 31 (1983).

[4]P. Cortona, S. Doniach, and C. Sommers, Phys. Rev. A **31**, 2842 (1985).

[5]H. Ebert, P. Weinberger, and J. Voitlander, Phys. Rev. B **31**, 7557 (1985); **31**, 7566 (1985).

[6]J. Staunton, B. L. Gyorffy, and P. Weinberger, J. Phys. F **10**, 2665 (1980).

[7]P. Weinberger, A. Gonis, A. J. Freeman, and A. M. Boring, Phys. Rev. B **31**, 1971 (1985).

[8]M. E. Rose, *Relativistic Electron Theory* (Wiley, New York, 1961).

[9]J. S. Faulkner, Prog. Mater. Sci. **27**, 73 (1982).

[10]P. Weinberger, J. Staunton, and B. L. Gyorffy, J. Phys. F **12**, 2229 (1982).

[11]P. Weinberger and A. Gonis, *Handbook on the Physics and Chemistry of the Actinides* (unpublished).

[12]Y. Onodera and M. Okazaki, J. Phys. Soc. Jpn. **21**, 2400 (1966).

[13]R. Dirl, R. W. Hasse, P. Herzig, P. Weinberger, and S. L. Altmann, Phys. Rev. B **32**, 788 (1985).